

A New Approach for Early Detection of PCB Pad Cratering Failures

Anurag Bansal, Gnyaneshwar Ramakrishna and Kuo-Chuan Liu
Cisco Systems, Inc.,
San Jose, CA
anurbans@cisco.com

Abstract

Pad cratering refers to the initiation and propagation of fine cracks beneath BGA pads in organic substrates or printed circuit boards. These cracks, which usually initiate under the application of excessive mechanical loads, represent a serious reliability concern for the industry. In typical board level reliability tests, solder joint failures are detected by an increase in electrical resistance of a daisy chain circuit followed by failure analysis. However, board level testing to determine the onset of BGA pad cratering has been problematic because the early stage of this failure mode is not associated with an electrical signature. Based on the mechanism of pad cratering, it is known that the cracks initiate beneath BGA pads and grow under continually increasing stresses until the pad completely separates from the substrate and a pad “crater” is formed. The catastrophic fracture of an interconnect, which causes an electrical “open”, is in fact the final and most catastrophic stage of the failure. At present the higher strain levels based on electrical resistance monitoring are being reported and used in design practices.

In this study, a new monitoring approach based on acoustic emission has been introduced for early detection of pad cratering failure. Two different lead-free daisy chain test vehicles were used with 1.0 mm pitch HSBGA-1096 and 0.8 mm pitch CABGA-160 packages, and four-point bend tests were performed to induce pad cratering. Acoustic emission activity from the test vehicles was monitored along with the electrical resistance of the daisy chain circuit. The bend test results, in conjunction with failure analysis, have shown that acoustic emission monitoring is indeed an effective methodology to detect the onset of the pad cratering. In contrast, the electrical daisy chain failure was detected at significantly higher strain. Using the acoustic emission approach, it has been found that PCB pad cratering failures can initiate at strain levels significantly lower than previously reported. This board level test methodology may now be used to evaluate the propensity of different materials and packages to pad cratering, and also to improve back-end manufacturing processes without using daisy chain test vehicles.

Introduction

The term “pad cratering” refers to the formation of fine cracks underneath BGA pads either in the PCB laminate material or in organic package substrates. Figure 1 schematically depicts the possible location of these cracks. Due to external mechanical load, the cracks initiate due to stress concentrations arising from the corner of the copper pad and the material property mismatch between copper and the laminate resin. The cracks propagate within the resin, up to the point where the underlying glass fiber bundles are encountered. Under subsequent loads, the cracks continue to grow along the interface between the resin and glass fibers, and also beyond the glass fiber bundle. Prior studies have shown that the extent of crack growth under the BGA pads is highly dependent on the location and orientation of glass fiber bundles with respect to the BGA pad [1].

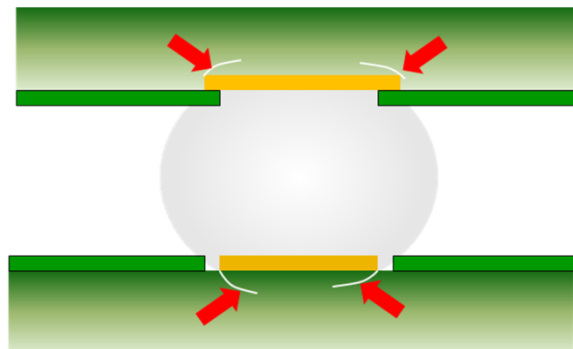


Figure 1 - Schematic Depiction of Pad Cratering

Pad cratering is a serious concern because depending on the loading conditions, the cracks can act either as a source for instantaneous catastrophic failure or as latent defects that can affect long term reliability. The ongoing industry transition to lead-free assemblies has further magnified this concern due to several factors. The higher reflow temperature involved in

lead-free assembly causes higher residual mechanical stress at the BGA pad interfaces [2]. The Sn-Ag-Cu (SAC) solder alloys, which are significantly stiffer and more brittle than eutectic tin-lead alloys, transmit higher stress to the BGA pads under a given mechanical load. The high T_g Phenolic-cured laminate materials used in Pb-free compatible PCBs are inherently more brittle than Dicy-cured laminates used in Sn-Pb assembly [3, 4]. Additionally, the trend of increasing device density and assembly miniaturization leads to the use of finer pitch components with smaller pad dimensions. The smaller pad dimensions are more susceptible to pad cratering under relatively lower mechanical loads [2].

The occurrence of internal laminate cracks under the BGA pads has mostly been observed under excessive monotonic or cyclic mechanical bending loads under quasi-static or dynamic (i.e., shock) conditions [1, 5-7]. These types of loads can be encountered during in-circuit testing (ICT) and PCB handling operations. Long *et al* have reported that pad craters due to excessive mechanical loads can cause electrical failures either due to the ultimate fracture of a trace connecting to the BGA pad, or due to cracking of a via located directly under the BGA pad [2]. Mukadam *et al* evaluated the long term reliability risk of existing laminate cracks. They reported up to 20% growth in pad cratering cracks under thermal cycling conditions [8]. Recently, Ma *et al* have even reported pad cratering as the primary failure mode in BGA test vehicles subjected to accelerated thermal cycling tests conducted with a wide temperature range of -55 to +125 °C [9]. Some studies have speculated that in the presence of moisture and electrical bias, internal pad cratering cracks can accelerate the conductive anodic failure (CAF) mechanism in PCBs [8]. At present it appears that the effect of pad cratering cracks on electrical signal integrity has not been studied.

In order to characterize the relative propensity of laminate materials for pad cratering, a pad pull test methodology has been developed and is presently being drafted as IPC standard 9708 [3, 4]. While the pad level pull test is useful for the relative grading of different laminates, the need for a board level test methodology has been highlighted in order to establish PCB strain limits in assembly and handling operations [2, 10, 11]. In typical board level reliability tests associated with solder joint fractures, an open circuit or increase in electrical resistance is conveniently used to detect the onset of failure. Due to the lack of an appropriate methodology for pad crater detection, several studies have continued to rely on an electrical resistance monitoring to characterize pad cratering. However, based on the nature of this mechanism, it is clear that the early stage of failure, i.e., the initiation of resin and intra-laminar cracks under the BGA pads, is not associated with an instantaneous change in electrical resistance. Under continually increasing loads, these cracks will grow to cause a trace fracture which causes an electrical event and the entire failure in its totality is characterized as a pad “crater”. Therefore the failure strains based on a change in electrical resistance are in-fact representative of the final and most catastrophic stage of this failure. At present these higher strains are being reported and used in design practices. To overcome this problem, some studies have attempted to establish strain limits by subjecting PCB assemblies to incrementally increasing load levels and then performing destructive failure analysis to check for the existence of pad craters [1, 11].

In this study, a new approach based on acoustic emission monitoring is being introduced for early detection of PCB bending induced pad cratering failure. Four point bend tests have been performed on daisy chain BGA test vehicles per IPC-9702 [12]. Acoustic emission sensors have been mounted on the boards to monitor acoustic activity, which is used as a way to detect the initiation of resin and intra-laminar cracks. In addition the electrical resistance of the daisy chain circuit has been monitored to detect the final catastrophic stage of failure.

Acoustic Emission

Acoustic Emission (AE) refers to the spontaneous release of transient elastic waves due to a sudden redistribution of stress in a material. When a structure is subjected to internal damage which can be caused by an external stimulus such as a change in pressure, load, or temperature, the localized damage will trigger the release of energy, in the form of acoustic/stress waves, which propagates in a radial direction from the source and is recorded by sensors. This technique has been used for decades to monitor the initiation and growth of cracks, slip and dislocation movements, metal twinning, and phase transformations. Acoustic emission monitoring is routinely used to monitor the integrity of pressure vessels and concrete structures. In composite materials, matrix cracking, fiber breakage and delamination contribute to acoustic emissions [13]. A schematic representation of a typical AE waveform is shown in Figure 2, superimposed with the key parameters that are used to define an AE “hit”. Additional details on the applications, parameter definitions, and waveform processing techniques may be found in the literature [13].

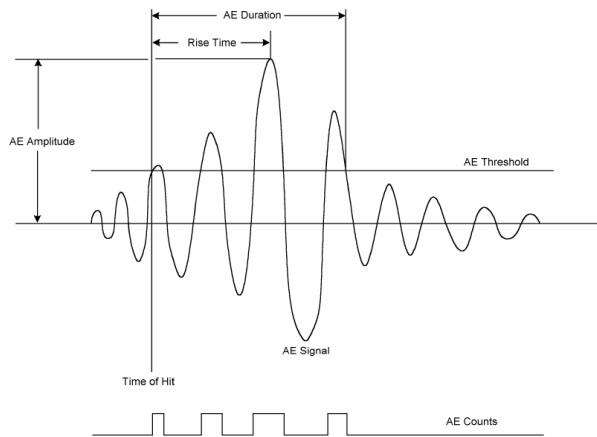
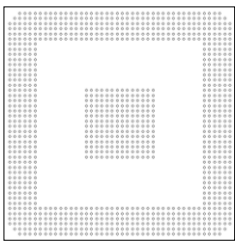
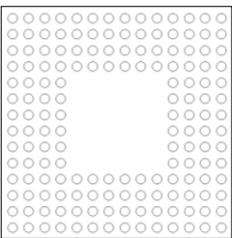


Figure 2 - Typical Acoustic Emission Waveform and Related Parameters [14]

Bend Test Methodology

Four point bend tests were performed according to IPC-9702 using daisy chain BGA test vehicles. The daisy chain packages were HSBGA-1096 with 1.0 mm pitch, and CABGA-160 with 0.8 mm pitch. Both packages consisted of organic BT substrate. Table 1 lists additional details of the test vehicles. The IPC-9702 method specifies tests to be carried out at high strain rates (> 5000 $\mu\text{e/s}$) in order to maximize the probability of generating brittle solder joint fractures at the intermetallic (IMC) layer. However, in the case of pad cratering, there is no evidence to suggest that these failures will only occur at high strain rates. Therefore, in this study the tests were conducted at both slow and high speed to characterize the effect of strain rate on pad crater initiation.

Table 1 - 4-Point Bend Test Vehicles

| Parameter | HSBGA 1096 | CABGA 160 |
|--------------------------|---|---|
| Pitch | 1.0 mm | 0.8 mm |
| Body Size | 45 mm x 45 mm | 12 mm x 12 mm |
| BGA Pad | 0.48 mm SMD | 0.4 mm, SMD |
| BGA Finish | Electrolytic Ni/Au | Electrolytic Ni/Au |
| Solder Composition | SAC405 | SAC305 |
| Solder Ball Diameter | 0.6 mm | 0.45 mm |
| PCB Size | 190 mm x 100 mm | 160 mm x 50 mm |
| PCB Finish | OSP | OSP |
| PCB stack-up / thickness | 8-layer, 93 mil | 8-layer, 93 mil |
| PCB Pad Size | 0.48 mm NSMD | 0.4 mm NSMD |
| PCB Laminate | Standard Pb-free compatible, $T_g = 180\text{ }^\circ\text{C}$ | |
| BGA Footprint |  |  |

The AE system used in this study had auxiliary data acquisition channels capable of acquiring analog data at a rate of 100 Hz. One channel was used to acquire the displacement output from the universal testing machine. Another channel was used to monitor the daisy chain continuity of the BGA package. This was accomplished by connecting one terminal of the daisy chain to a D.C. power supply in constant current mode and monitoring the voltage change. As shown in Figure 3, a single axis 120 Ohm resistance strain gage was mounted on 12 boards for each package type (i.e. 6 boards each, tested at slow and high speed). The strain gage was located on the secondary side of the board and directly under the location of the corner-most BGA joint where the highest strain concentration is expected. The gage size and specifications were according to the guidelines in IPC-9702.

During the bend tests, two acoustic emission sensors were clamped on the ends of the PCB, as shown in Figure 3. The sensors were connected to the AE monitoring system via a preamplifier. The acoustic data acquisition rate for both sensors was 10 MHz. Figure 4 shows a picture of the HSBGA board during test.

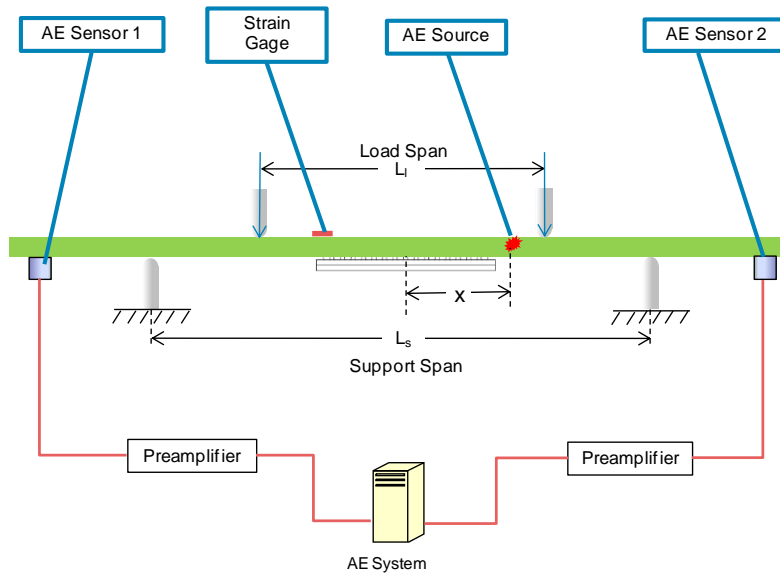


Figure 3 - Schematic of Bend Test Set-up with AE Sensors



Figure 4 - Four Point Bend Testing of HSBGA board

The acoustic emission test set-up required careful optimization of several parameters that are used to process the raw acoustic wave and record acoustic “counts”, “hits” and “events” [13, 14]. The main objective behind optimization of these AE system settings was to ensure that all valid events in the vicinity of the BGA package are accurately recorded, while ensuring that spurious signals such as background noise, universal testing machine vibrations, and frictional contact at the load and support anvils are not recorded. In order to establish these parameters, a 0.5 mm diameter mechanical pencil was used and a series of pencil lead break (PLB) tests were carried out on test boards. The PLB test is widely used in acoustic emission testing, where the pencil lead break at a given location is used as a simple means of generating known acoustic waves in the test sample in order to optimize AE system settings [15]. The optimized value of some of the key parameters for this test is shown in Table 2. In addition to detecting the acoustic events generated during the bend tests, with the use of two sensors located at each end of the PCB, it was possible to linearly locate the source of the AE events. In order to do this, a series of PLB tests were performed at predetermined locations on a test board and the velocity of sound travelling through the PCB material was determined as

$$v = \Delta x / \Delta t \quad (1)$$

Where, Δx is the difference in the proximity of the PLB location to sensors 1 and 2, and Δt is the time difference between the detection of the PLB event at sensor 1 and sensor 2. As shown in Table 2, it was found that the optimized empirical velocity of sound was different in the HSBGA and CABGA boards. Referring to Figure 3, if an AE event occurred during the actual bend tests, the position x of the AE source could be linearly located as

$$x = v \times \Delta t \tag{2}$$

Table 2 - Bend Test Parameters

| System | Parameter | HSBGA 1096 | CABGA 160 |
|-----------|-------------------------------------|---------------|-----------------|
| Bend Test | Load Span (L_l) | 100 mm | 50 mm |
| | Support Span (L_s) | 150 mm | 100 mm |
| | Crosshead Speed | 1.0, 6.5 mm/s | 0.6, 4.0 mm/sec |
| AE System | Sensor Diameter | 10 mm | |
| | Sensor Frequency | 300 KHz Max | |
| | Noise Threshold | 50 dB | |
| | Number of Hits per Event | 2 | |
| | Acoustic Data Acquisition Frequency | 10 MHz | |
| | Analog Data Acquisition Frequency | 100 Hz | |
| | Preamplifier Gain | 40 dB | |
| | Speed of Sound, v | 3.06e+06 mm/s | 3.5e+06 mm/s |

AE Source Location Calibration

Once the velocity of sound within the PCBs was determined, PLB tests were performed in order to determine the accuracy of linear source location. The pencil leads were broken at pre-determined locations on the board and the AE system was used to detect the x-location. Figures 5 and 6 show the PLB test results for the HSBGA and CABGA boards respectively. The absolute energy of the signal is shown along the y-axis, and the x-location is shown on the x-axis. In order to account for the possibility of acoustic wave attenuation and secondary wave reflection from the fixture anvils, the tests were conducted with the board placed within the fixture and applying a preload to ensure good contact between the anvils and the board. A schematic of the BGA package, the loading and supporting anvils, and the sensor locations have been superimposed for convenience.



Figure 5 - Linear Source Location Using PLB Test for HSBGA Boards

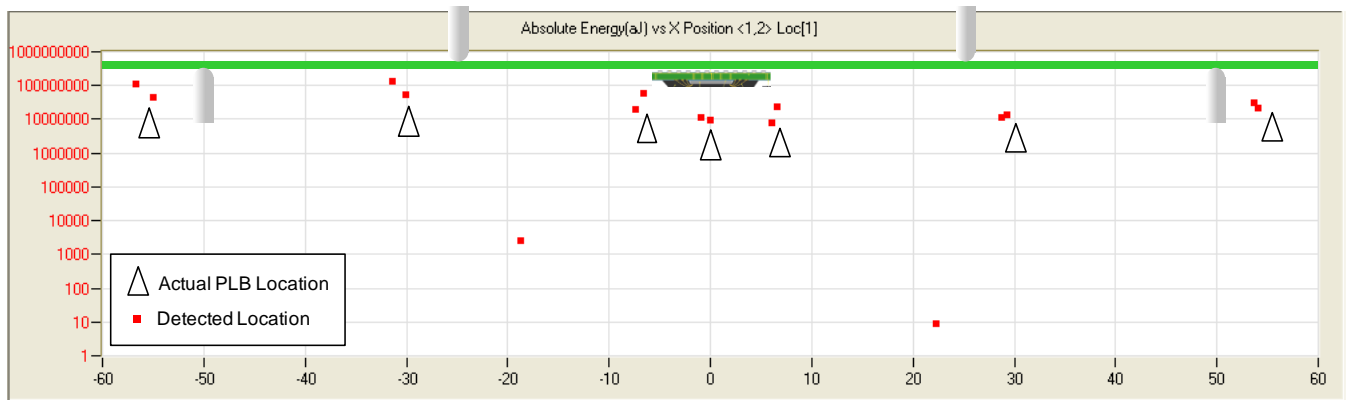


Figure 6 - Linear Source Location Using PLB Test for CABGA Boards

Upon comparison of the actual PLB locations and the locations detected by the AE system, it is estimated that the detected x-locations are accurate in the range of ± 1 mm at or near the package edge, ± 2 mm near the loading anvils, and ± 3 mm near the supporting anvils. This result is consistent with the expectation from equation (2) that the accuracy of the linear location (x) will be better if the source is located near the center of the board, resulting in a small Δt value.

Bend Test Results

Figures 7 and 8 show the data acquisition results during the bend testing of a typical HSBGA and CABGA board. Figure 7 (a) shows the cross-head displacement and electrical voltage output versus time. Figure 7 (b) shows the Absolute Energy of AE hits detected by sensors 1 and 2 during the test. Figure 7 (c) shows time on the y-axis and the detected linear location on the x-axis. The AE events were based on detection of a hit by both sensor 1 and 2, and the linear location was calculated by the difference in the time when the two sensors detected a hit (equation 2). A schematic of the test board dimensions along with the loading and supporting anvils has been included for reference. It can be seen that after the start of the bend test, there is a duration of “quiet period” during which no AE hits were detected. This demonstrates that, with the AE system settings used in the test, no spurious signals were being recorded due to the frictional contact between the anvils and the test board. At a well defined instant in time, the “quiet period” ends due to a significant extent of AE activity, as indicated by the onset of the first AE hit and first AE event. The linear location plot shows that the initial AE events were primary located near the left and right edge of the package. This demonstrates additional validation that the initial AE events being detected were indeed emanating from damage being induced near the solder joints, and not due to activity near the fixture anvils. With the progression of time, a significant number of high energy AE hits were detected, and the linear location of the AE events shifted from the package edges towards the center of the package and the entire length of the board. The electrical resistance of the daisy chain circuit rapidly increased during this stage, indicating a catastrophic failure in the circuit. This trend, which was consistently seen in all of the boards tested, clearly demonstrates that the onset of electrical failure of the daisy chain circuit occurs very late after a significant extent of damage has been accumulated at the solder joints. In contrast, the acoustic emission methodology is able to adequately detect the onset of damage at the solder joints. This is validated by the finding that no spurious hits were detected during early stages of the test and the source of the first few hits was located near the package edges.

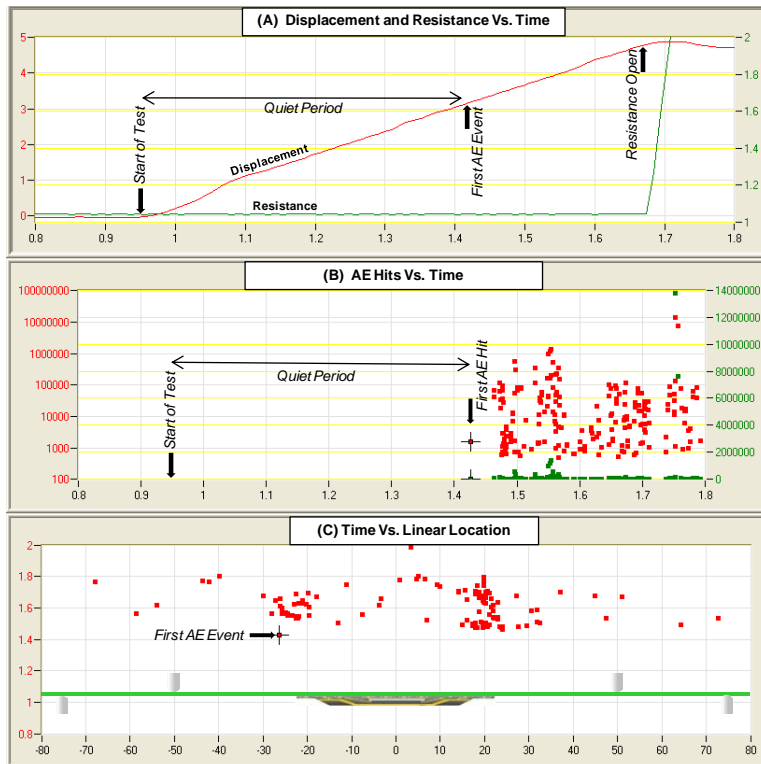


Figure 7 - Bend Test Result of a Typical HSBGA board

Similar to the HSBGA results, Figure 8 shows the same results and trends during bend testing of a typical CABGA board. Once again, there was a well defined “quiet period” during which no high energy hits or events were detected. Once the AE events were detected, the source of these events was clearly identified near the left and right edges of the package. With further progression of time, the source of AE activity spread towards the center of the package and eventually to the entire

length of the board until an electrical open circuit was detected due to rupture of a copper trace. In the case of CABGA boards, the gap between the onset of AE activity and electrical failure was much more significant than the HSBGA boards.

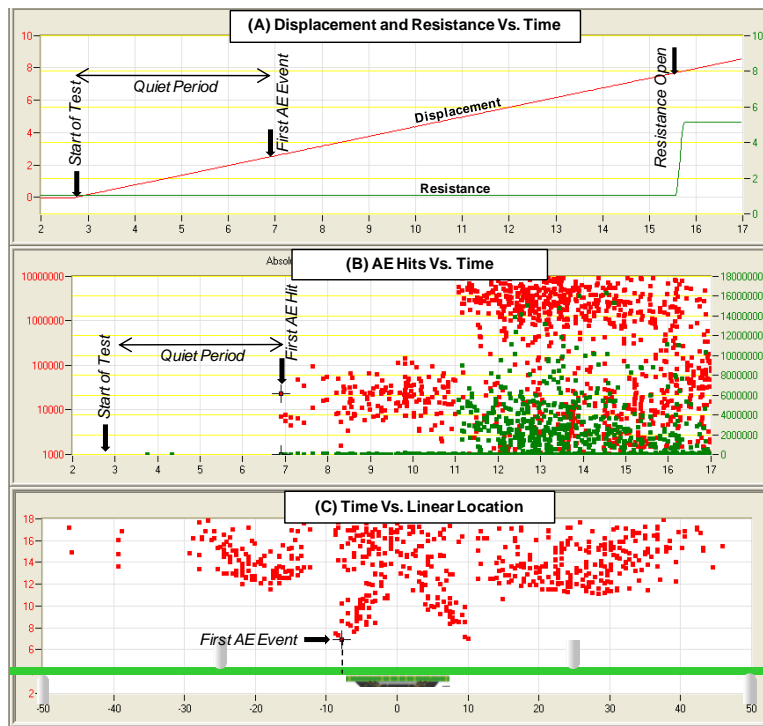


Figure 8 - Bend Test Result of a Typical CABGA board

During the bend test, single axis strain gages were mounted on several boards. The strain gages, placed on the secondary side directly beneath the corner-most solder joint location, were used to determine the maximum strain on the board. Figure 9 shows the strain response from several HSBGA and CABGA boards tested at slow and fast cross-head speed. For the HSBGA boards, the strain rates were 1200 microstrain per second ($\mu\epsilon/s$) and 8000 $\mu\epsilon/s$. For the CABGA boards, the strain rates were 850 $\mu\epsilon/s$, and 5700 $\mu\epsilon/s$. Since there was good correlation in the strain results, the strain versus displacement relationship was established and used to determine the strain in boards that did not have strain gages attached.

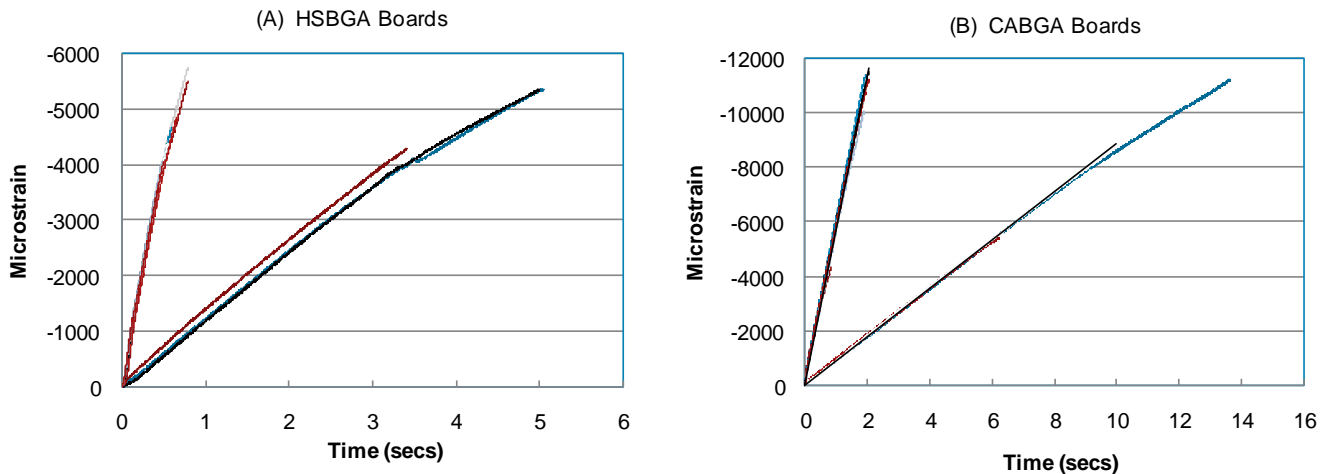


Figure 9 - Strain vs. Time Relation for HSBGA and CABGA Boards

The PCB strains at the onset of failure determined by AE events and electrical failure are shown in Figure 10 for HSBGA boards. Note that in some cases the bend tests were terminated before any electrical failure occurred, hence the electrical failure strains for those boards were not shown in Figure 10. It is evident that the failure strains based on AE activity are significantly below the failure strains at the onset of electrical failure. Furthermore, the effect of strain rate on at the AE failure strain was not statistically significant, although the average failure strain was somewhat lower in the high speed tests and there was more scatter in the results with slow speed testing.

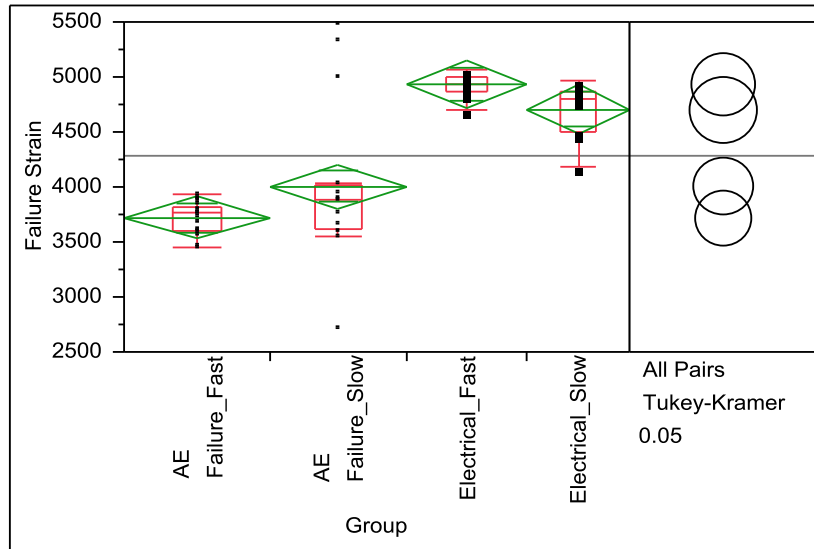


Figure 10 - AE and Electrical Failures of HSBGA Boards

Figure 11 shows the failure strains at the onset of failure determined by AE activity and electrical failure of CABGA boards. In this case, the gap between the failure strains based on AE activity and electrical failure was even more significant. The electrical failure occurred at 3X higher strain than failures detected by AE. Also, the effect of strain rate was statistically significant for the AE failure. The high speed tests had AE failure at lower strains. The effect of strain rate was insignificant for the onset of electrical failure.

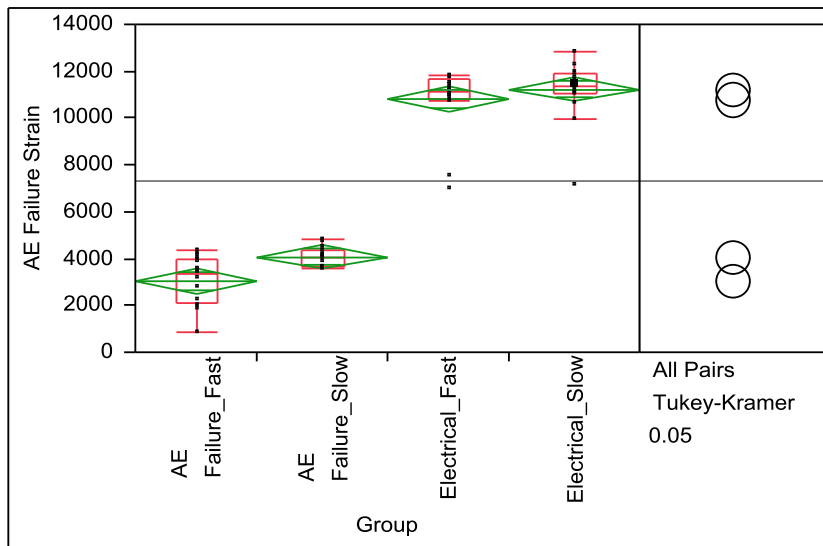


Figure 11 - AE and Electrical Failures of CABGA Boards

Failure Analysis

Dye and Pry and cross-sections were performed on selected test boards to ascertain the failure modes. The linear source location data from the AE system was used to determine which side of the package encountered the first failure, and the first row of solder joints along this side was cross-sectioned. All the failures in the HSBGA and CABGA test vehicles were found to be due to initiation of pad cratering cracks on the PCB side. Figure 12 shows SEM cross-sections from HSBGA boards where the bend testing was terminated at three different stages. Figure 12 (a) shows a typical joint from a board tested at slow speed up to a peak strain of 5000 $\mu\epsilon$, and no high energy AE events or electrical failure was detected. Both sides of the HSBGA were cross-sectioned, and no pad cratering damage was observed. In this board, only 2 out of 80 solder joints observed had evidence of very minor shearing between the fiber bundles oriented at 0 and 90 degrees. This type of damage could easily be introduced in sample preparation or polishing. Figure 12 (b) shows a typical solder joint cross-section of another HSBGA board in which AE failure was recorded at 3900 $\mu\epsilon$, and the test was terminated at 4000 $\mu\epsilon$ without any

electrical failure. Pad cratering was clearly evident in several solder joints along the edge of the package. As expected, the cracks originated at the PCB pad corner and propagated into the resin until the first layer of glass fiber bundles was encountered. Figure 12 (c) shows typical solder joints along the edge of a HSBGA board tested at high speed. In this case AE failure was recorded at 3900 μe , electrical failure occurred at 4300 μe , and the test was terminated at 4400 μe . It is clear that in this board, where electrical failure was recorded, the failure had progressed to a significantly more advanced stage resulting in complete tearing away of the PCB pads and rupturing of copper traces connecting to the pads.

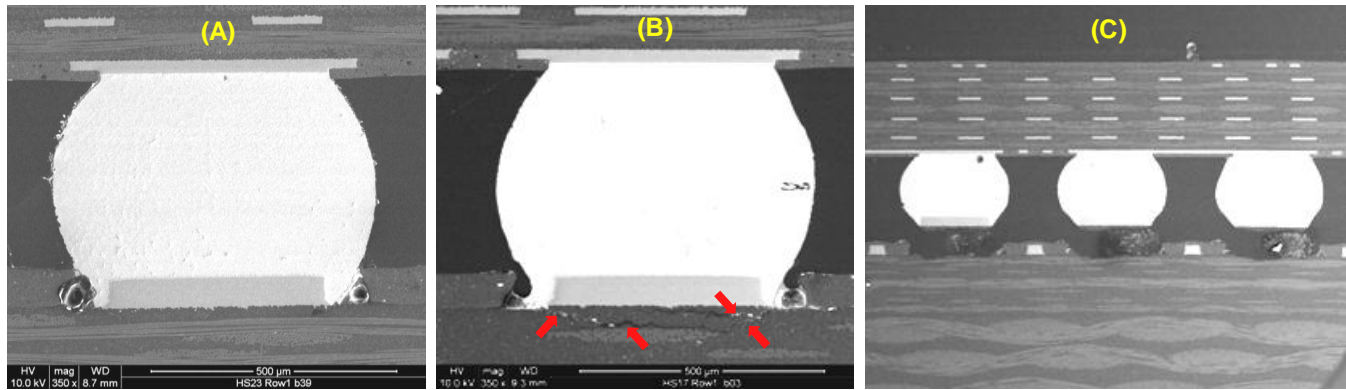


Figure 12 - HSBGA board cross-sections (a) No AE Failure or Electrical Failure, (b) AE Failure but no Electrical Failure, and (c) AE and Electrical Failure

In the case of the CABGA boards, all of the tested boards had recorded AE failure, but several boards did not reach electrical failure. Figure 13 shows a typical solder joint cross-section along the edge of the package. This board was tested at slow speed, AE failure was recorded at 4000 μe , there was no electrical failure and the test was terminated at 7000 μe . Once again several solder joints had clear evidence of pad cratering on the PCB side.

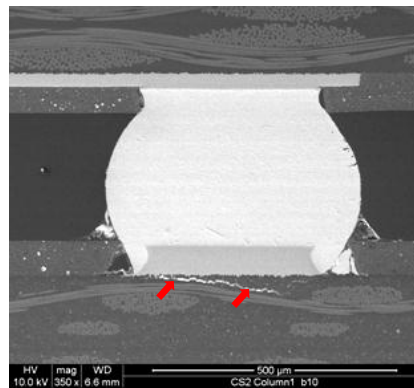


Figure 13 - Typical CABGA Cross-section with AE Failure but no Electrical Failure

Discussion and Future Work

The results presented thus far have shown that acoustic emission, associated with the spontaneous release of elastic energy during four point PCB bend tests, can be successfully monitored. Spurious AE events due to background noise or frictional contact are not being detected because there is a significant “quiet period” during the initial stages of PCB bending. Once the AE activity begins, the events being detected have relatively high absolute energy, and linear source location has shown that the initial AE events are in fact emanating from the edges of the BGA package. Failure analysis has been conducted on selected boards and the results have shown that in the case where the test was terminated without detection of any high energy AE events, there was no sign of pad cratering along both edges of the package. In cases where the tests were terminated after detection of high energy AE events, but without reaching electrical failure, several BGA pads had pad cratering at the PCB side. The cross-sections of boards which encountered both AE failure and electrical failure revealed a very late stage in the evolution of pad cratering damage. In these boards the entire pad was seen to have torn off the PCB and the package was visibly lifted from the board. Based on these results, it is evident that acoustic emission monitoring can indeed serve as a convenient methodology for detecting the onset of pad cratering damage.

As noted in the introduction, the lack of a suitable board level test methodology to detect the onset of pad cratering has been a significant barrier for determining the PCB strain limits.

The failure strains based on electrical resistance monitoring will significantly overestimate pad cratering resistance, and should therefore not be used to determine strain limits for actual PCB assembly, test, and handling operations. With use of the AE method, we can now see that the failures are initiating at significantly lower strain levels and by fitting an appropriate distribution it should be possible to establish the true strain limits. Figure 14 shows Weibull distributions for AE failure and electrical failure in the HSBGA boards. Since the effect of strain rate was statistically insignificant for the AE failures, the high speed and slow speed results have been combined. Using a 1% failure limit, it can be seen that the PCB strain limit to prevent pad cratering failures should be approximately 2500 $\mu\epsilon$.

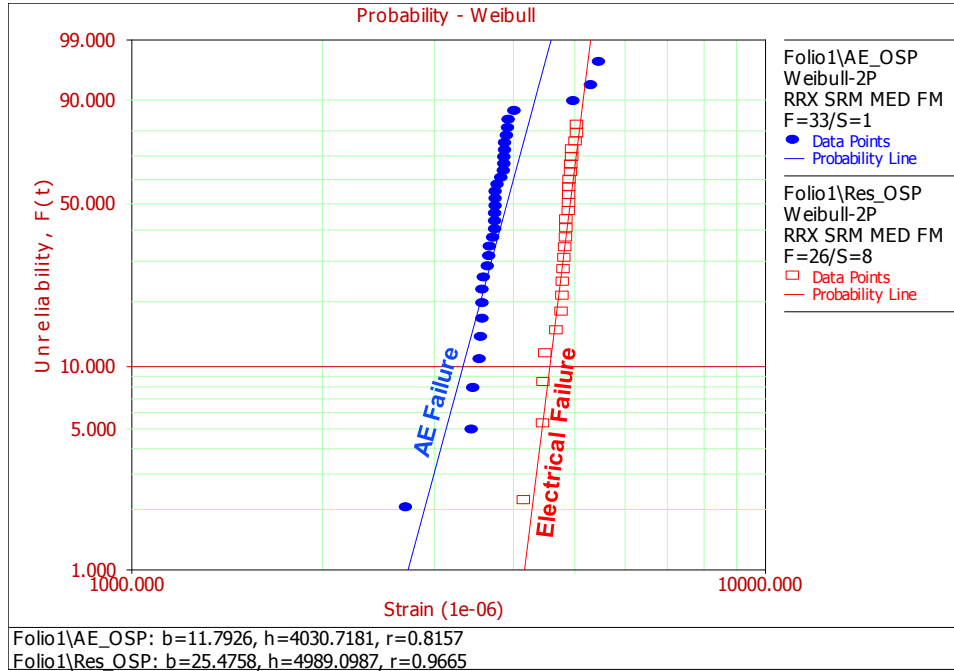


Figure 14 - Weibull Distribution Plot for HSBGA AE and Electrical Failure

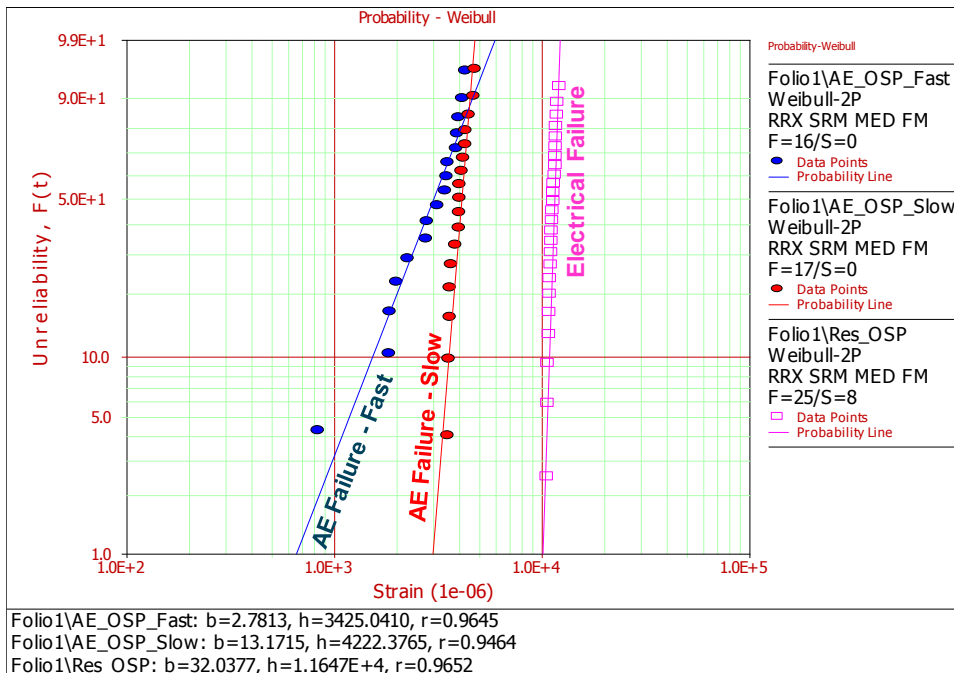


Figure 15 - Weibull Distribution Plot for CABGA AE (Slow, Fast) and Electrical Failure

For the CABGA boards, the Weibull distributions for AE failure and electrical failure are shown in Figure 15.

In this case the effect of strain rate was statistically significant (for AE failures) hence the distributions at slow and high speed testing have been separated. Based on a failure limit of 1%, the PCB strain limit under high strain rate will be approximately 650 $\mu\epsilon$. The lower strain limit in high strain rate tests may be due to the increased stiffness of the Sn-Ag-Cu solder under high strain rate conditions, which will transfer higher stress to the PCB pad [16]. Since these types of packages have significantly delayed electrical failures, in the past small plastic BGAs were incorrectly assumed to be at low risk for pad cratering. The results in this study clearly show that the effect of the smaller pad size is very significant. Therefore in spite of a smaller package size and relatively lower package stiffness, the CABGA packages have a considerably lower PCB bending strain limit.

The development of the AE methodology, and the initial findings presented in this study, has several far reaching implications as discussed below.

- (i) The most significant finding is the realization that PCB pad cratering failures will initiate at strain levels significantly below those reported in prior studies which were based on electrical resistance monitoring. The small and flexible 0.8 mm pitch CABGA package is at higher risk for pad cratering than the stiffer and larger body size 1.0 mm pitch HSBGA package. This suggests that the effect of a smaller BGA pad size is very significant.
- (ii) The AE methodology does not rely on electrical signals for detection of failures hence the use of custom designed daisy chain test vehicles will not be necessary for determining PCB strain limits for pad cratering. This could represent significant cost savings for characterization of mechanical robustness of solder joints and PCB laminate materials. In future these tests may be performed with dummy or non-functional components.
- (iii) While the present study focused on PCB pad cratering failures, there are several other failure mechanisms that may not be electrically detectable and could be investigated by the AE approach. For example, the onset of brittle solder joint fractures in power and ground pins, which are often located at BGA package corners are expected to generate relatively high energy acoustic events. Other failure mechanisms could be solder joint fractures in passive components, MLCC capacitor cracking, delamination in components or PCBs, and die cracking.
- (iv) In addition to PCB bending tests, it is possible that the acoustic monitoring approach may be extended to detect onset of damage in other types of board level environmental stress tests such as thermal cycling, mechanical shock, or vibration. It is certainly expected that some of these tests will pose a greater challenge in eliminating background noise from the test.
- (v) The bend test vehicle used in this study had a relatively simple design. In future it is conceivable that more advanced acoustic monitoring techniques could be developed to debug mechanical damage in functional PCB assemblies with significantly higher complexity in design and density.

Conclusions

A board level acoustic emission monitoring method has been developed as a means for detecting the onset of pad cratering failures in PCB bending tests. Using this approach, the board level strain limits for PCB bending in assembly, test, and handling operations can be determined at different strain rates. Based on the acoustic method, the PCB strains at the onset of pad cratering were found to be significantly lower than prior expectations, which were based on electrical failure of daisy chain circuits. In comparison with a larger and stiffer 1.0 mm pitch HSBGA package, a smaller and more flexible 0.8 mm pitch CABGA package was found to have a significantly lower strain limit. This implies that the effect of a pad size is a significant variable and finer pitch BGA components should be considered at high risk for pad cratering. Pad cratering failures were found to be relatively independent of the strain rate in HSBGA packages, but the smaller CABGA packages had a lower pad cratering strain limit at high strain rates.

Acknowledgements

The authors gratefully acknowledge the help of Tam Dam and Cherif Guirguis in conducting the tests. Thanks are also due to the Interconnect Technology Team members at Cisco Systems, Inc. for their help and valuable suggestions. We also wish to thank Ron Miller of Mistras Group for his expert advice on the acoustic emission testing aspects of this work.

References

- [1] G. Godbole et al, "On The Nature of Pad Cratering", Proc. 59th Electronic Components and Technology Conference (ECTC), (2009)
- [2] G. Long et al, "Lead Free Assembly Impacts on Laminate Material Properties and "Pad Crater" Failures", IPC APEX Conference, (2007)
- [3] M. Ahmad et al, "Comprehensive Methodology To Characterize and Mitigate BGA Pad Cratering in Printed Circuit Boards", Jl. of Surface Mount Technology, Vol. 22, Issue 1, Jan-Mar, (2009)

- [4] M. Ahmad et al, "Validated Test Method To Characterize And Quantify Pad Cratering Under BGA Pads On Printed Circuit Boards", IPC/APEX 2009 Conference, Las Vegas, NV, April, (2009)
- [5] A. Bansal et al, "Comparison of Substrate Finishes for Flip Chip Packages", Electronic Components and Technology Conference (ECTC), (2005)
- [6] A. Bansal et al, "Flexural Strength of BGA Solder Joints with ENIG Substrate Finish using 4-point Bend Test", JI. Of Surface Mount Technology, Vol. 18 #2, (2005)
- [7] A. Bansal et al, "Modeling and Experimental Correlation of BGA solder joints under PCB bending", SMTA Intl. Conference, (2006)
- [8] M. Mukadam et al, "Impact of Cracking Beneath Solder Pads in Printed Circuit Boards on Reliability of Ball Grid Array Packages", SMTA Intl. Conference, (2005)
- [9] H. Ma et al, "Acceleration Factor Study of Lead-Free Solder Joints under Wide Range Thermal Cycling Conditions", Electronic Components and Technology Conference (ECTC), (2010)
- [10] D. Xie et al, "Failure Mechanism and Mitigation of PCB Pad Cratering", Electronic Components and Technology Conference (ECTC), (2010)
- [11] B. Gray et al, "Mechanical Failures in Pb-free Processing: Selected Mitigation Techniques for Pad Crater Defects", SMTA Intl. Conference, (2010)
- [12] IPC/JEDEC 9702, "Monotonic Bend Characterization of Board Level Interconnects"
- [13] "Acoustic Emission Testing", Nondestructive Testing Handbook, 2nd Edition, Vol. 5, American Society for Nondestructive Testing, Inc., (1987)
- [14] PCI-2 Based AE System User's Manual, Rev. 3, Physical Acoustics Corporation, April 2007
- [15] "Standard Guide for Determining the Reproducibility of Acoustic Emission Sensor Response", ASTM Standard E976 – 10, ASTM International, West Conshohocken, PA, DOI: 10.1520/E0976-10
- [16] H. Ma, "Effects of Temperature and Strain Rate on the Mechanical Properties of Lead-Free Solders", JI. Of Materials Science, vol. 45, (2010)